Low-temperature anharmonicity and symmetry breaking in the sodalite $|Na_8I_2|[AlSiO_4]_6$

Lars Robben[a,b]*, Isaac Abrahams[c], Michael Fischer[d], Stephen Hull[e], Martin T. Dove[f] and Thorsten M. Gesing [a,b]

a) University of Bremen, Institute for Inorganic Chemistry and Crystallography, Leobener Str. 7, D-28359 Bremen, Germany

b) University of Bremen, MAPEX Centre for Materials and Processes, Bibliothekstrasse 1, D-28359 Bremen, Germany

c) School of Biological and Chemical Sciences, Queen Mary University of London, Mile End Road, London E1 4NS, United Kingdom

d) University of Bremen, Crystallography Group, Department of Geosciences, Klagenfurter Str. 2-4 ,28359 Bremen, Germany

e) ISIS Facility, Rutherford Appleton Laboratory, Chilton, Didcot, Oxfordshire OX11 0QX, United Kingdom

f) School of Physics and Astronomy, Queen Mary University of London, Mile End Road, London E1 4NS, United Kingdom

Abstract

The aluminosilicate iodide sodalite $|Na_8I_2|[AlSiO_4]_6$ was examined by temperature-dependent neutron time-of-flight powder diffraction from 5 K to 290 K and X-ray diffraction from 298 K to 1200 K. The temperature-dependent properties of the mean structure in space group $P\bar{4}3n$ were obtained by Rietveld analysis. A negative slope for the thermal expansion coefficient below 50 K could be observed, and the displacement parameters of the iodide ions indicate anharmonic effects. Local structure models ($8 \times 8 \times 8$ super cells) were refined against pair-distribution functions calculated from total scattering data collected at 5 K, 165 K and 240 K. The results indicate isotropic displacements for all atoms except for I-atoms, showing the effects of an anharmonic potential around this anion at very low temperatures.

Introduction

Anharmonicity in materials is one of the frontier topics in materials research [1]. It is the cause of thermal expansion [2] and thus its technical importance, e.g. for thermal-energy conversion, is obvious. In thermal-energy conversion, where parasitic heat conduction by phonons in solid-state compounds is the physical basis for Peltier and similar effects [1], anharmonicity gives rise to the thermoelectric effect [3], which is nowadays even more relevant in the light of the global energy and climate change challenges [4,5]. Anharmonicity at elevated temperatures (i.e. well above 300 K and near to a material's melting point) is a general phenomenon often considered in calculations by using Buckingham or similar potential functions. However, at low temperatures potential functions are in most cases assumed to be harmonic. Recently, low-temperature anharmonicity in CsCl was observed by Sist and co-workers [6]: This well-known compound shows anharmonicity in the Cs atoms displacement parameters at 20 K.

Sodalites are the simplest zeolites and are built up of a 3-dimensional network of corner-sharing MO_4 tetrahedra (where M could be eg. Al^{3+}, Ga^{3+}, Si^{4+}, Ge^{4+}, see [7]), forming the so-called ***sod***-cages, containing extra-framework cations and templating ions. Sodalites show great variability in their composition; a comprehensive overview is given by Fischer and Baur [7,8]. The highest possible symmetry for sodalites is space group $Im\bar{3}m$ (aristotype), observed in pure silica sodalites [9,10]. Nevertheless, more than half of all known sodalites crystallize in space-group $P4\bar{3}n$. In this space-group the highest possible symmetry is reduced due to alternating occupation of the framework cations by pairs of atoms (like Al-Si, Ga-Ge, Al-Ge, Ga-Si, Zn-P). The high flexibility of the sodalite framework due to the tilt-mechanism [11], allows also the encapsulation of various templating ions. The combination of framework composition and template ion determines the sodalite's room temperature unit cell size, thus systematic variation of either the framework atoms or the template ions could give insight in the nature of the template-framework interactions. Research considering the thermal

expansion of sodalites started with the work of Taylor [12], examining the thermal expansion of sodalites, noseans and haüynes from 298 K to 1193 K. This work was continued for a range of synthetic sodalites in which sodium was exchanged by lithium and potassium [13] or the halide anion was varied [14]. In all these studies, the description of the thermal expansion was carried out in a phenomenological way with polynomial functions. Hassan et al. [15] presented temperature-dependent synchrotron X-ray measurements on the aluminosilicate chloride sodalite, $|Na_8Cl_2|[AlSiO_4]_6$, from 301 K to 1255 K and concluded that the driving force for the thermal expansion and the structural behaviour is the expansion of the Na-Cl bond length in the sodalite cage forcing the framework to expand. The tilting of the framework is the structural response of the framework to increased temperature and the degree of tilting is essentially correlated with the room-temperature unit cell size [16].

Low-temperature (i.e. below 300 K) studies of sodalites are rare [17] and mostly concentrate on the silica sodalite with its pure SiO_2 framework and organic molecules inside the cage (e.g.[18]). These compounds show indications of phase transitions in this temperature range, but the full elucidation of the structural changes remains an unsolved problem [10]. Kashiwagi et al. [19] examined the antiferromagnetic resonance in $\left|Na^{+I}{}_6Na^0{}_2\right|[AlSiO_4]_6$ by electron spin resonance (ESR) and observed a small anisotropy field of $2 \cdot 10^{-5}$ T, as well as a distinct change in the shape of the ESR signal below 40 K. The authors concluded that this may be caused by small deviations from the cubic structure at very low temperatures.

In this study, we present a detailed examination of the thermal behaviour of aluminosilicate iodide sodalite by neutron and X-ray scattering methods from 5 K to 1200 K. The calculated temperature-dependent thermal expansion (TEC) coefficients indicate an anomalous thermal expansion below 50 K. The obtained displacement parameters were modelled numerically and anharmonic effects in the displacement parameters of the iodine atoms are evident. Refinements of structure models against pair distribution functions obtained from total scattering data give insight into the local structural order in this system.

Experimental Details

The aluminosilicate iodide sodalite $|Na_8I_2|[AlSiO_4]_6$ (Na-I-SOD) was synthesised hydrothermally under autogeneous pressure in a 50 ml Teflon-lined steel autoclave. The autoclave was filled with a gel prepared from 5 g sodium iodide, 1.2 g Na_2SiO_3, 0.8 g $NaAlO_2$ and 20 ml 8 M NaOH and heated for 48 h at 473 K. After cooling to ambient temperature, the product was filtered, washed several times with distilled water and dried at 353 K.

Neutron powder diffraction (ND) data were obtained on the Polaris diffractometer at the ISIS Facility, Rutherford Appleton Laboratory, United Kingdom. Data were collected on backscattering (average angle 146.72°), 90° (average angle 92.59°), intermediate angle (average angle 52.21°), low angle (average angle 25.99°) and very low angle (average angle 10.40°) detectors, corresponding to the approximate *d*-spacing ranges 4-260 pm, 5-410 pm, 7.3-700 pm, and 13-1380 pm and 30-4800 pm, respectively. Measurements were carried out with the sample contained in a cylindrical 11 mm diameter vanadium can, placed in a He-cryostat located in front of the backscattering detectors. Data were collected at selected temperatures from 5.1(1) K to 290 K. At 5.4(1) K 19 measurements of total proton beam current of 10 μAh were obtained and subsequently summed. Total proton beam current of 30 μAh data sets were collected at higher temperatures. Data for an empty vanadium can (ca. 600 μAh) collected under identical conditions to the sample were used for data correction.

The temperature-Odependent X-ray powder diffraction (TD-XRD) data were collected on a PANAlytical X'Pert PW3373 diffractometer equipped with an Anton Paar HTK1200N temperature chamber, using Cu-K_α radiation ($\lambda_{K\alpha1}$ = 154.05929(5) pm, $\lambda_{K\alpha2}$ = 154.4414(2) pm), a secondary Ni-filter and an X'Celerator multi-strip detector. All measurements were carried out in the 2θ range from 10° to 130°, with a step width of 0.0167° and a total measuring time of 76 s per step. Diffraction patterns were recorded in 25 K steps over the temperature range from 298 K to 1273 K.

All scattering data were modelled in batch mode using the Rietveld method (TOPAS V4.2, Bruker AXS, Karlsruhe, Germany), taking the results of a refinement as starting values for the next higher temperature step. For the TOF data profile parameters were fitted to a Si standard sample for all detector banks and fixed in the sample refinements. The starting model was taken from Nielsen et al. [20]. The fundamental parameters were fitted against a LaB_6 standard material. During the refinements, the average crystal size ($L_{Vol}(IB)$) and the contribution of the micro-strain (ε_0) to the reflections were refined as well as lattice, isotropic displacement and the variable atomic position parameters. The Si-O distances were constrained to 164 pm.

Total scattering analysis of ND measurements at 5 K, 165 K and 240 K were carried out by calculation of the pair distribution function (PDF) using the software Gudrun [21]. This software was used for data merging, correction of the scattering contributions of the sample environment as well as for the data normalization. A triclinic 8 × 8 × 8 sodalite supercell based on the respective average structure refinement was the starting model for the PDF fitting with RMCprofile [22]. Fitting was carried out against the total normalized scattering *S(Q)* and the total pair correlation function *D(r)*, as well as the Bragg profile data to provide a constraint for the long-range crystallinity. *S(Q)* data were broadened by convolution with a box function to reflect the finite size of the simulation box.

Ab-initio MD calculations were performed using the CP2K code (version 2.4.0, installed on Hochleistungsrechenzentrum Berlin), which permits MD calculations in the framework of density-functional theory (DFT) using a mixed Gaussian and plane wave basis [23,24]. The calculations employed the PBE functional, and used an energy cutoff of 400 Ry.[25] Goedecker-Teter-Hutter pseudopotentials optimized for the PBE functional [26] were combined with the DZVP-SR (double-zeta plus polarisation – short range) basis from the series of molecularly optimized basis sets developed by Van de Vondele and Hutter [27]. The ab-initio MD calculations were carried out for the following temperatures: T = 298 K, 598 K

and 998 K. Prior to the calculations, the structure of Na-I-SOD was optimized using DFT, fixing the lattice parameters to the experimental values for the respective temperatures.

Molecular Dynamics (MD) calculations using empirical force field parameters were carried out using the GULP code (version 4.3) included in the DS Biovia Materials Studio software [28]. The force field parameters for silicon, aluminium, oxygen, and sodium were taken from the collection of shell-model potentials based around the oxygen-oxygen potential developed by Catlow and co-workers (Si-O, O-O: [29], Al-O, Na-O: [30]). Parameters for the interaction between iodine atoms, and between iodine and sodium, were taken from the work of Catlow, Diller, and Norgett [31]. To model all relevant interaction between different atom types, the Buckingham potential parameters for the iodine-iodine interaction from that work were also used for iodine-oxygen interactions. A 2 × 2 × 2 supercell of the sodalite unit cell was used and the calculations were performed in the canonical ensemble, using the Nosé-Hoover thermostat to control the temperature. Using a time-step of 0.5 fs, an equilibration stage of 1.5 ps was followed by a production stage of 3.5 ps. The obtained trajectories were used to calculate the mean atomic positions and displacement parameters (Figure S6, Table S3), and in the case of the force-field MD calculations, the average kinetic energy for each atom (Table S3).

Results

The average sodalite structure and its thermal behaviour

The structure at 5.4(1) K could be refined in space group $P\bar{4}3n$ with a lattice parameter a = 899.651(3) pm using the structural parameters given by Nielsen [20] as starting values in the refinement. The resulting R_{wp} = 1.56% indicates a very good fit (Figure 1) and the validity of the average structure model (structure and refinement parameters and fitted diffraction profiles are given as supplementary information S1). Analysis of the variable temperature data revealed no unexpected behaviour (see supplement S2). The lattice expansion causes a continuous reduction of the framework tilt angle and at T_C = 1023(2) K a tri-critical phase transition from space-group $P\bar{4}3n$ to the fully expanded state in space-group $Pm\bar{3}n$ occurs (for details see supplement S2).

Thermal Expansion

The thermal expansion coefficients, $\alpha_{I,vol}(T_m)$ and $a^*_{I,vol}(T_2)$, were calculated from James et al. [32]:

$$\alpha_{I,vol}(T_m) = \frac{1}{V_0} \cdot \frac{V_{n+1} - V_n}{T_{n+1} - T_n}; T_m = \frac{T_{n+1} + T_n}{2} \quad (1)$$

and

$$a^*_{I,vol}(T_n) = \frac{1}{V_0} \cdot \frac{V_n - V_0}{T_n - T_0} \quad (2)$$

where V_0 is here the cell volume at 5 K; T_{n+1}, T_n and V_{n+1}, V_n are the temperatures and cell volumes of the data sets $n+1$ and n. The definition of the TEC used in Equation 2 is unusual, but shows some interesting sample behaviour below 50 K, which could not be seen well in the TEC calculated according to equation 1 (Figure 2 a), due to high scattering of the data points. The TEC $\alpha_{I,vol}(T_M)$ (Figure 2 b) shows distinct features between 200 K and 250 K and

around 500 K and 1000 K. The change in the TEC around 1000 K is associated with the $P\bar{4}3n \leftrightarrow Pm\bar{3}n$ phase transition at 1023(2) K. The feature around 500 K fits very well to the temperature range in which Fechtelkord observed an increase in the Na mobility in this compound [33] and may tentatively be attributed to such an effect. Another important observation is that the general slopes of the TEC are distinctively different above and below 250 K. The TEC $a^*_{I,vol}(T_2)$ (only data points below 300 K are shown in Figure 2 c) shows a distinct feature around 250 K in the $\alpha_{I,vol}(T_M)$ as a linear offset. At 40 K, this TEC reaches zero K^{-1} and changes slope at lower temperatures. The lattice volume expansion and the TEC $\alpha_{I,vol}(T_M)$ were fitted by a Debye-model and $a^*_{I,vol}$ could be calculated from the model volume (red line in Figure 2 c). The quasi-harmonic Debye model cannot explain the observed features below 40 K and between 200 K and 250 K. A Debye temperature for the data below 300 K of 509(10) K was obtained from this model (for details see supplement S-3).

The atomic displacement parameters

The temperature dependency of the displacement parameter of a certain atom $\langle u_{iso}\rangle^2(T)$ can be described by the general formula:

$$\langle u_{iso}\rangle^2(T) = c_a + D_a(T) + A_a(T) \quad (3)$$

where c_a is a constant describing the contribution from zero-point-energies and atomic disorder, $D_a(T)$ is a harmonic approximation of the displacement parameter and $A_a(T)$ is a function describing the high-temperature anharmonicity of the atom a. A temperature-dependent harmonic approximation of the displacement parameter factor was given by Guinier (see p. 191 in [34]):

$$D_a(T) = \frac{424}{M_a} * \frac{T}{\theta_{Da}} * \left[\frac{1}{4}\frac{\theta_{Da}}{T} + \frac{T}{\theta_{Da}}\int_0^{\frac{\theta_{Da}}{T}} \frac{y\,dy}{e^y - 1}\right],$$

(4)

with θ_{Da} denoting the specific Debye-temperature for the atom *a* with atomic mass M_a and *T* being the temperature. The Debye-function $\frac{T}{\theta_{Da}}\int_0^{\frac{\theta_{Da}}{T}}\frac{y\,dy}{e^y-1}$ with its integration variable *y*, was integrated numerically and its value determined by a polynomial approximation $f\left(\frac{\theta_{Da}}{T}\right)$. Equation 4 assumes independent atoms without any bonding interactions. However, as shown below, this approximation can work well for atoms bonded with strong covalent contributions, if an additional parameter, *b*, is included describing the individual bonding contributions to give an effective atomic mass, M_a^{eff} (equation 5):

$$M_a^{eff} = M_a \cdot b$$

(5)

Using this approach, movement restrictions of the atoms due to harmonic bonding potentials are taken into account in *b*. High-temperature anharmonic effects are approximated by an anharmonicity constant, c_{Aa} within $A_a(T)$[35]:

$$A_a(T) = c_{Aa} * \left(\frac{\theta_{Da}}{T}\right)^{-4}$$

(6)

The overall trend in the displacement parameters is at first glance consistent with the temperature increase using a fixed value of 1 for parameter *b*. Keeping this in mind, fitting of the temperature dependency of the displacement parameters was carried out initially for the low temperature TOF data to determine c_a and $D_a(T)$. With fixed c_a and Debye-temperature, θ_{Da}, the anharmonicity term was refined against the full data, using at the same time an additional linear offset factor to shift the values obtained by X-ray diffraction to those from the neutron data. Due to the poor scattering contrast between Al and Si in the X-ray measurements, the *B*-values of the two atoms were constrained together in an additional refinement.

Calculating the average Debye-temperature by a weighted mean of the individual atomic values [36] leads to a value that is approximately 150 K larger than the one calculated from the volume-expansion. Using equation 3, with a free atomic *b* parameter and setting $c_a = 0$ for Al, Si, O and Na leads to an excellent fit, with *b* greater than 1. However, using the same approach for iodine yields a *b* value of less than 1, reflecting a much weaker interaction between iodine and the other atoms in the system, thus *b* was fixed to 1 in this case. The fitting results are shown in Figure 3, the parameter values are collected in Table 1.

The dynamic behaviour of the average structures was investigated using molecular dynamic calculations, based on force-fields and density functional theory. The trajectories obtained by those calculations were used to determine the temperature-dependent kinetic energies of the different atoms. Details of these calculations and the results are given in the supporting information (see SI-4). The determined kinetic energies of the iodine ions are used to assess the Na-I interaction at very low temperatures (see section "discussion").

The local structure at 5 K, 165 K and 240 K

At selected temperatures (5 K, 165 K and 240 K) TOF data were collected with an extended measurement time to improve the signal-to-noise-ratio. The data were corrected, normalized and in each case the *D(r)* function was calculated.

The average structure obtained from the Rietveld refinement at each respective temperature was used to generate an 8 × 8 × 8 super cell with 23552 atoms in space group $P1$, which was used as a starting model in fitting the *D(r)* function by varying the atomic positions, resulting in excellent fits to the data (see Figure 4).

To evaluate the structural features of these models, the absolute difference vectors between the atomic positions $\vec{X}$ in the starting model (denoted by index 0) and the end configuration (denoted by index E) were calculated:

$$\vec{D}_N = \overrightarrow{X_0} - \overrightarrow{X_E} \tag{7}$$

Sorting these values according to the respective atomic sites, the shift with respect to sites in the average structure in space group $P\bar{4}3n$ is obtained (see SI-5). The center of gravity for a crystallographic site can be calculated by:

$$\vec{C} = \frac{1}{N}\sum_{N}\overrightarrow{D_N} \tag{8}$$

with N being the number of atoms of one crystallographic site. Assuming a Gaussian distribution, the components u_{ij} of the anisotropic displacement tensor for each atom could be calculated using the standard deviations σ_i of each coordinate i of $\vec{D}_N$ and the covariance (cov) by:

$$u_{ij} = \begin{cases} i = j: \sigma_i^2 \\ i \neq j: cov(x_i, x_j)\sigma_i\sigma_j \end{cases} \tag{9}$$

The equivalent isotropic displacement parameter is calculated using the average of the main axis components. The values of these parameters are collected in Table 2.

Discussion

Structural and dynamical aspects of the sodalite structure

The two different approaches, Rietveld refinement of the Bragg scattering and Reverse Monte Carlo fitting of the total scattering data, generate the time- and space averaged structure and the time-averaged local structure, respectively. They differ in the model size. In the first case, the displacement parameters contain the dynamical aspects of the structure as well as structural disorder. In the second case, the degree to which the structural disorder can be elucidated depends on the data resolution and the computational power limiting the model size, but the model gives a distribution of the possible average positions of the atoms. To get comparable numbers from each model, the Gaussian distribution of the difference vectors has

been calculated and can be compared with the displacement parameters from the Rietveld refinements (Figure 5). This comparison shows that for sodium and oxygen the structural disorder is always smaller than the dynamical disorder. For silicon, the structural disorder at 240 K lies on the displacement parameter fit and the dynamical disorder is lower than the structural disorder for lower temperatures. In the case of aluminum, the structural disorder can be estimated to become larger than the dynamical disorder between 160 K and 200 K, for iodine the same effect is observed below 50 K. It is significant that the temperatures at which the structural disorder of Al, Si and I become larger than the dynamical disorder correlate well with the temperatures where anomalies are observed in the TEC.

Therefore, the offset in the volume TEC between 160 K and 240 K could be explained by the following mechanism. When the structural disorder of the silicon atoms is larger than the dynamical disorder (this could be described as a freezing process), the other atoms in the framework move to their mean positions to maintain equilibrium bond distances. Because of the dynamical nature of Al and O in this temperature range, the volume expands slightly. Then the Al atoms also freeze, and they will do so at equilibrium bond distances determined by the disordered silicon positions. The volume then relaxes to the expected value.

The local environment of iodine

The above calculation of the structural displacement parameters assumes a Gaussian distribution of the difference vectors. Plotting these vectors around their crystallographic sites gives spherical distributions (as expected for a Gaussian distribution) around the respective crystallographic sites (see SI-5) for all atoms except iodine. Plotting the temperature-dependent volume density of iodine atoms in 10 contour levels between one and the maximum number of iodine atoms per volume element (Figure 6) shows distinct changes of the distribution with temperature: The 240 K distribution shows a tetrahedral shape, with the tips of the distribution pointing towards the 6-ring windows where no sodium atoms are located; the distribution is deformed and contracts slightly with decreasing temperature. The

inner part of this distribution (leaving out the 1 atom/voxel contour) shows a homogeneous distribution for 165 K and 240 K, whereas the distribution at 5 K is strongly elongated along the x-axis. A cubic distortion of this volume can be calculated by considering the deviations of the observed edge lengths from the edge length of a cube of equivalent volume. The mean values and the standard deviations of these deviations are shown in Figure 7. For 165 K and 240 K the cubic distortions are 0.09(4) and 0.08(4), respectively, at 5 K the distortion increases by almost a factor of three to 0.25(19).

To obtain a possible explanation the local potential of the Na-I system can be analysed. In the average crystal structure model in space group $P\bar{4}3n$ iodine occupies the 2*a* position (0, 0, 0). The next neighbour of iodine is sodium on the 8*e* position (*x*, *x*, *x*) which coordinates the iodine tetrahedrally. The local potential U_{total} at a point *w* within this tetrahedron can be calculated using the superposition

$$U_{total}(\mathrm{w}) = \sum_{i=1}^{4} U_{iw} \tag{10}$$

of single Buckingham potentials (with *i* indicating the i^{th} Na atom):

$$U_{iw} = A \cdot e^{-\frac{r_{iw}}{\rho}} - \frac{C_6}{r_{iw}^6} \tag{11}$$

The parameters *A*, ρ and C_6 are the same as those used in the FF-MD calculations; r_{ix} is the distance between point *w* and the i^{th} Na atom. The calculation was carried out using the Na positions obtained at 5 K; all other energy contributions are neglected in this approach. Figure 8 shows energy isosurfaces (isosurfaces around the minimum are blue and around the maximum value are red) of U_{total} within the Na-I coordination tetrahedron. The calculated energy at the centre, the average crystallographic position of iodine, is 1.95(1) meV and the minimum potential energy in the cage is 2.53(3) meV approximately 300 pm away from the

centre in the directions of the main axes. The difference between these two points is about 0.6 meV. Using the approach that the energy of an atom is the sum of the kinetic and potential energies $U_{iodine} = U_{total} + U_{kin}$ it is clear that the distinct shape of U_{total} comes into effect as soon as the kinetic energy of the iodine is lower than the energy difference of 0.6 meV. Taking the kinetic energies estimated from FF-MD calculations (see SI-4 Table S3) and their temperature linearity, it can be calculated that below ≈ 20 K, E_{kin} becomes smaller than 0.6 meV and thus the potential low-energy shape comes into effect. As a direct consequence, the anharmonic potential surface at low energies is responsible for a local symmetry breaking of the average sodalite structure. The observed shape of the iodine distribution is elongated in one direction and from the presented calculation one could assume a distribution of the iodine atoms on two main minima in each main axial direction. This discrepancy could be explained by the highly idealized character of the potential calculation; the sodium positions are fixed and there are no contributions from the framework. In nature, it is easily conceivable that one minimum is preferred by distortions of the central potential due to small movements of the framework and thus of the sodium atoms to minimize their energy.

Summary and conclusions

A detailed study of the temperature-dependent behaviour of $|Na_8I_2|[AlSiO_4]_6$ through examination of the time and space averaged crystallographic structure and the time average local structure has enabled a separation of structural and dynamical effects.

The distribution of iodine atoms in the real structure follows the potential surfaces of the Buckingham potential between sodium and iodine. An important feature of this potential is the difference between the local maximum at the average crystallographic position of the iodine and the cage's local minimum. The reduction of the kinetic energy due to cooling forces iodine atoms to the minimum potential; away from the centre of the ideal ***2a*** site. This effect is not very pronounced, with the potential minimum lying within the ionic radius of

iodine (127 pm) around the (0,0,0) position. Nonetheless, this effect locally breaks the space group symmetry. Iodine can move on the minimum surface and experimentally this is reflected in the distribution of iodine atoms obtained from the RMC fitting of the PDF data. The effects of the reduced atomic kinetic energy are clearly visible in the presented anomalies in the TECs, which in future could be used for a quick check on such specific effects before investing time and effort into total scattering data collection and analysis.

Within this work we have elucidated the structural causes for the anomalies observed in the TEC and have shown that below 50 K anharmonic effects of the central cage potential have to be taken into account and a local symmetry breaking of the iodine takes place. Such effects may also explain the observation of an anisotropy field in $\left|\mathrm{Na}_6^{+1}\mathrm{Na}_2^{0}\right|[\mathrm{AlSiO_4}]_6$, a very closely related compound, below 20 K by Kashiwagi e.a. [19].

Acknowledgements

The authors gratefully acknowledge the STFC for funding the ISIS/Polaris measurements (Proposal number RB1220172) and the North-German Supercomputing Alliance (HLRN) for providing HPC resources that have contributed to the results reported in this paper. M. Fischer gratefully acknowledges funding by the Central Research Development Fund of the University of Bremen (Funding line 04 – Independent Projects for Post-Docs).

Notes and references

[1] J.P. Heremans, *Nat. Phys.* **2015**, 11, 990–991.

[2] H. Ibach, H. Lüth, Solid-State Physics: An Introduction to Principles of Material Science, **2003**.

[3] X. Shi, L. Chen, C. Uher, *Int. Mater. Rev.* **2016**, 61, 379–415.

[4] The United Nations: 2030 Agenda for Sustainable Development, New York, **2016**.

[5] The United Nations: Paris Agreement, New York, **2015**.

[6] M. Sist, K.F.F. Fischer, H. Kasai, B.B. Iversen, *Angew. Chemie - Int. Ed.* **2017**, 56, 3625–3629.

[7] R.X. Fischer, W.H. Baur, in:, R.X. Fischer, W.H. Baur (Eds.), Zeolite-Type Cryst. Struct. Their Chem. Framew. Type Codes RON to STI. Landolt-Börnstein - Gr. IV Phys. Chem. (Numerical Data Funct. Relationships Sci. Technol. Vol 14E., Springer, Berlin.

[8] R.X. Fischer, W.H. Baur, *Zeitschrift Für Krist.* **2009**, 224, 185–197.

[9] D.M. Bibby, M.P. Dale, *Nature* **1985**, 317, 157–158.

[10] J.W. Richardson, J.J. Pluth, J. V Smith, W.J. Dytrych, D. Bibby, *J. Phys. Chem.* **1988**, 92, 243–247.

[11] W. Depmeier, *Zeitschrift Fuer Krist.* **1992**, 89, 75–89.

[12] D. Taylor, *Miner. Mag* **1968**, 761–769.

[13] C.M.B. Henderson, D. Taylor, *Phys. Chem. Miner.* **1978**, 2, 337–347.

[14] T. Gesing, *Zeitschrift Für Krist.* **2007**, 222, 289–296.

[15] I. Hassan, S.M. Antao, J.B. Parise, *Am. Mineral.* **2004**, 89, 359.

[16] D. Taylor, *Miner. Mag* **1972**, 38, 593–604.

[17] S. Luger, J. Felsche, P. Fischer, *Acta Crystallogr. Sect. C Cryst. Struct. Commun.* **1987**, 43, 1–3.

[18] C.M. Braunbarth, P. Behrens, J. Felsche, G. van de Goor, *Solid State Ionics* **1997**, 101, 1273–1277.

[19] T. Kashiwagi, T. Nakano, A. Hanazawa, Y. Nozue, M. Hagiwara, *J. Phys. Chem. Solids* **2010**, 71, 544–547.

[20] N.C. Nielsen, H. Bildsoe, H.J. Jakobsen, P. Norby, *Zeolites* **1991**, 11, 622–632.

[21] A. Soper, *RAL Tech. Rep.* **2011**, RAL-TR-2011-013.

[22] M. Tucker, D. Keen, M. Dove, *Mineral. Mag.* **2001**, 65, 489–507.

[23] J. Vandevondele, M. Krack, F. Mohamed, M. Parrinello, T. Chassaing, J. Hutter, *Comput. Phys. Commun.* **2005**, 167, 103–128.

[24] J. Hutter, M. Iannuzzi, F. Schiffmann, J. Vandevondele, *Wiley Interdiscip. Rev. Comput. Mol. Sci.* **2014**, 4, 15–25.

[25] J.P. Perdew, K. Burke, M. Ernzerhof, *Phys. Rev. Lett.* **1996**, 77, 3865–3868.

[26] M. Krack, *Theor. Chem. Acc.* **2005**, 114, 145–152.

[27] J. VandeVondele, J. Hutter, *J. Chem. Phys.* **2007**, 127, 114105.

[28] J.D. Gale, A.L. Rohl, *Mol. Simul.* **2003**, 29, 291–341.

[29] M.J. Sanders, M. Leslie, C.R.A. Catlow, *J. Chem. Soc. Chem. Commun.* **1984**, 1271.

[30] R.A. Jackson, C.R.A. Catlow, *Mol. Simul.* **1988**, 1, 207–224.

[31] C.R.A. Catlow, K.M. Diller, M.J. Norgett, *J. Phys. C Solid State Phys.* **2001**, 10, 1395–1412.

[32] J.D. James, J.A. Spittle, S.G.R. Brown, R.W. Evans, *Meas. Sci. Technol.* **2001**, 12, 1–15.

[33] M. Fechtelkord, *Solid State Nucl. Magn. Reson.* **2000**, 18, 70–88.

[34] A. Guinier, X-Ray Diffraction in Crystals, Imperfect Crystals, and Amorphous Bodies, San Francisco, **1963**.

[35] A. Maradudin, P. Flinn, *Phys. Rev.* **1963**, 129, 2529–2547.

[36] A.C. Lawson, D.P. Butt, J.W. Richardson, J. Li, *Philos. Mag.* **2007**, 87, 2507–2519.

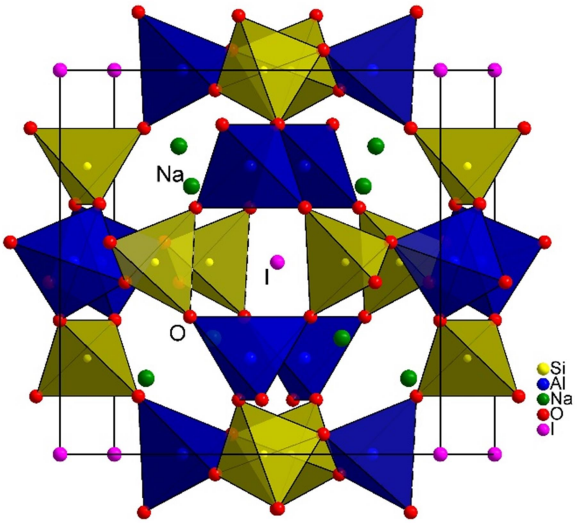

Figure 1: Average structure of $\left|Na_8I_2\right|[AlSiO_4]_6$ at 5 K

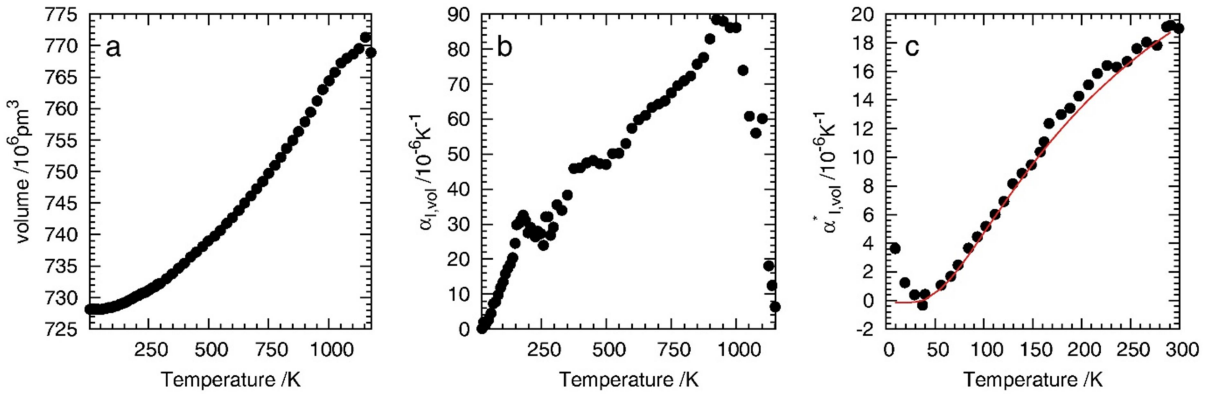

Figure 2: a: Thermal volume expansion ; b: TEC $a_{I,vol}$; c: $a^*_{I,vol}$ (only low temperature data) with the calculated values from the Debye fit (red line).

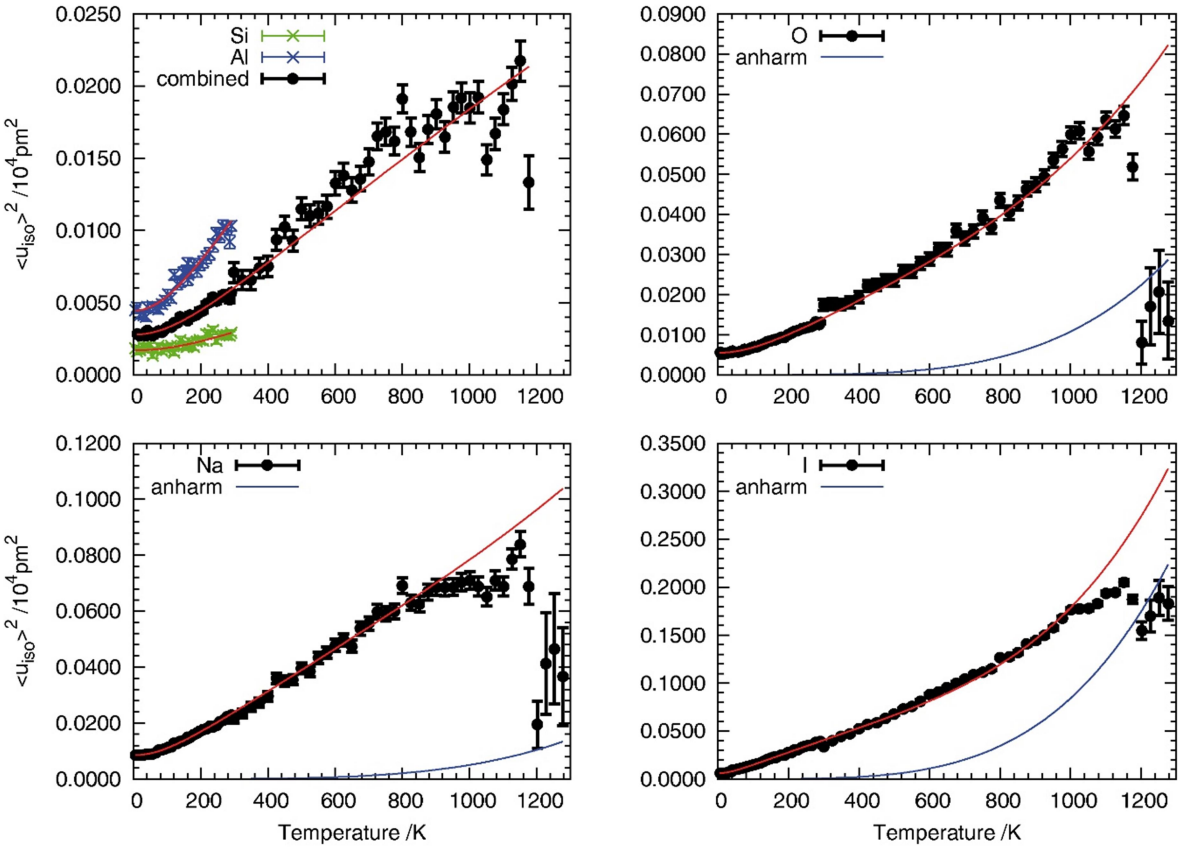

Figure 3: Temperature-dependent mean isotropic displacement parameters (Al and Si only distinguished using the low-temperature TOF data) along with the fit results according to equation 3 (red line) and the anharmonic high-temperature contribution (blue line).

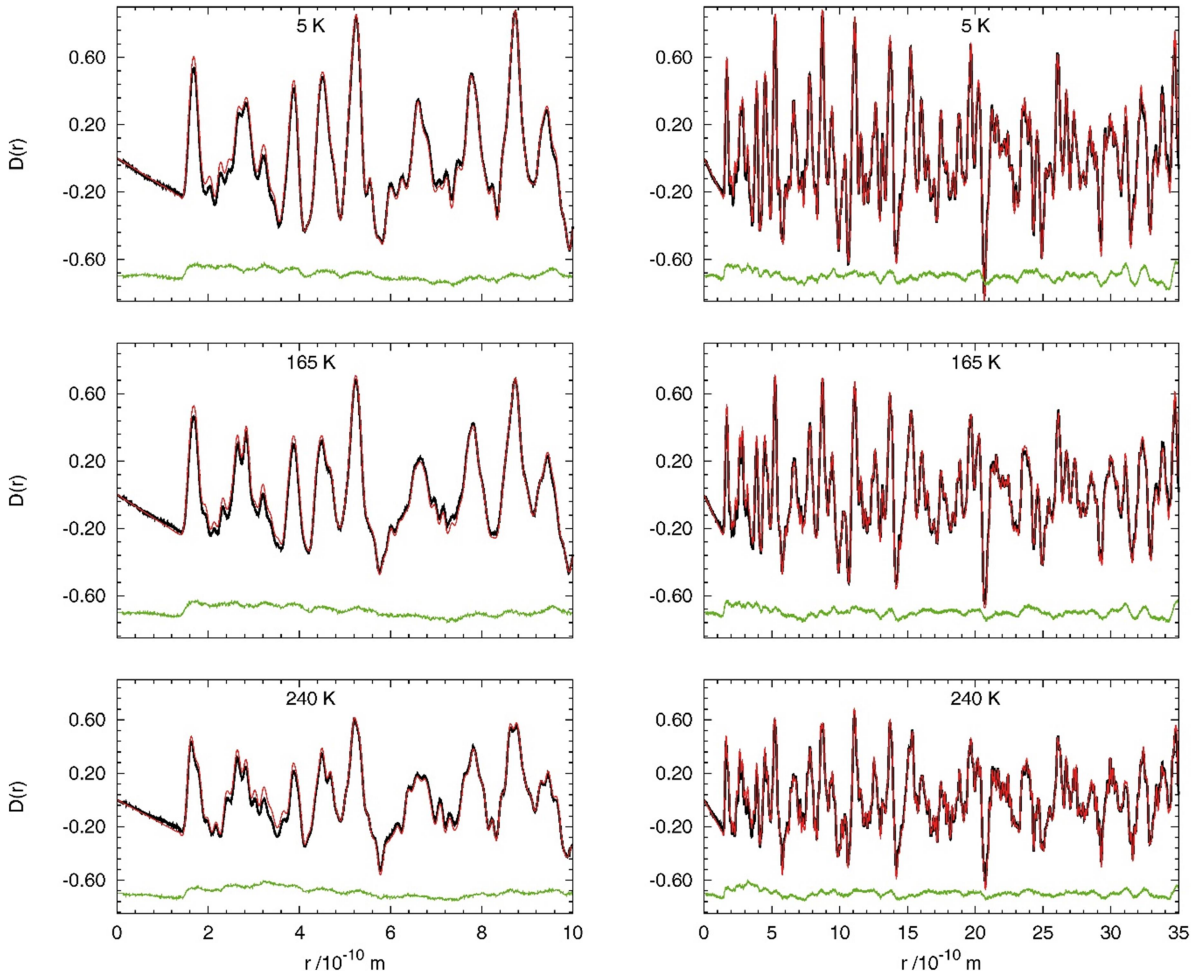

Figure 4: Pair distribution function refinement results. PDFs obtained from measured data (black), calculated *D(r)* (red) and difference curves (green, shifted for the sake of clarity) for the complete data (right) and enlargement of the range up to 1 nm ($10 \bullet 10^{-10}$ m).

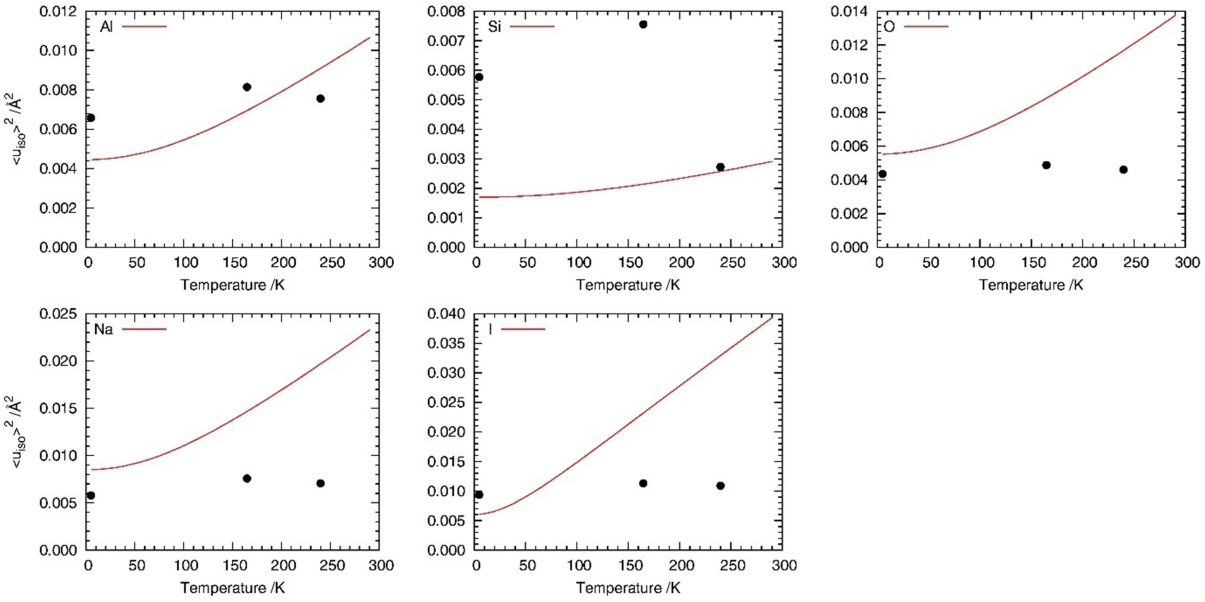

Figure 5: Comparison of the Debye-Waller-factor model fit (from Rietveld refinement results, red lines) with the isotropic structural displacement parameters obtained from PDF model fits (black points)

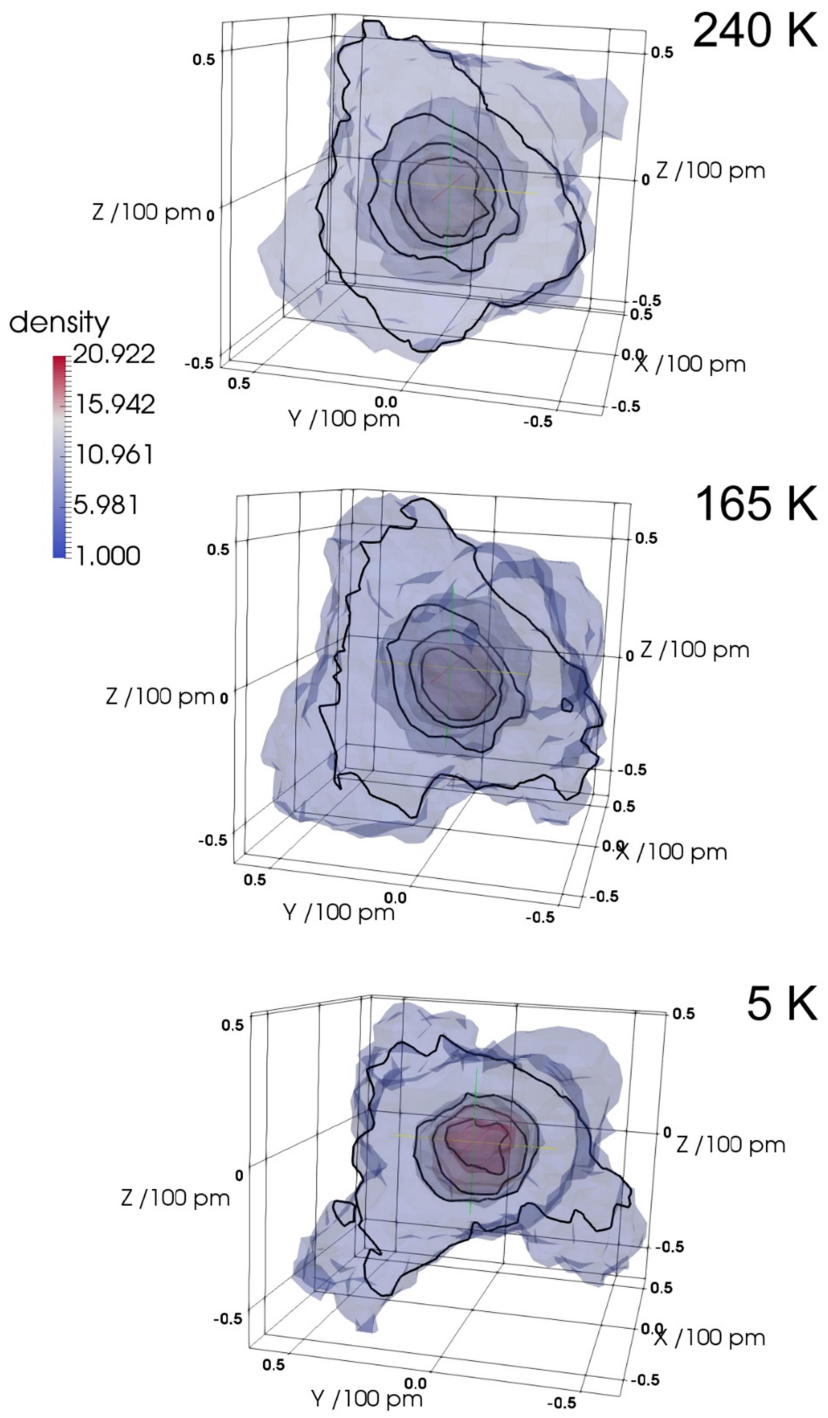

Figure 6: Volume density of iodine atoms obtained from the RMC calculations (detail see text). Density contour levels are given in the scale (minimum in all three cases: 1; maximum is for 5 K: 82, 165 K: 43 and 240 K: 36 atoms / voxel)

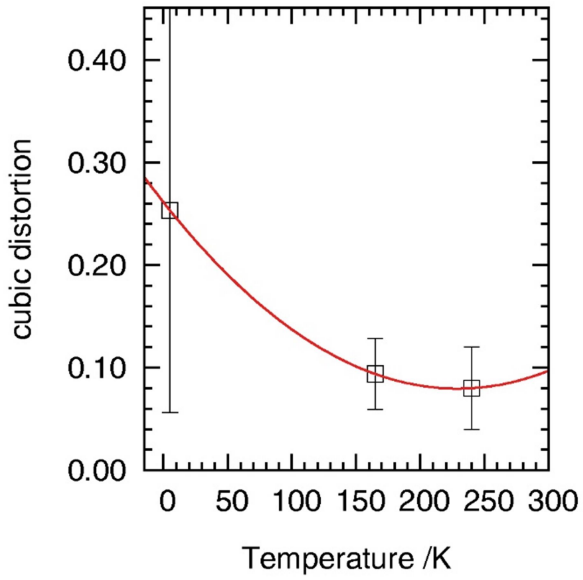

Figure 7: Cubic distortion of the innermost part of the iodine distribution shown in Figure 6. The red line is a quadratic polynomial as a guide for the eye.

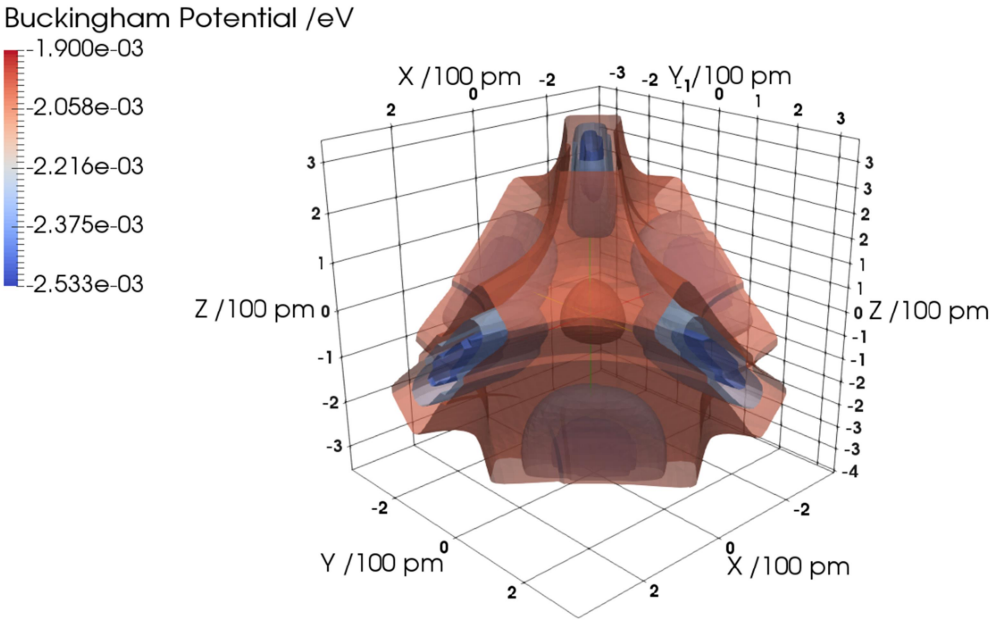

Figure 8: U_{total} energy isosurfaces of the Buckingham potential within the Na-I coordination tetrahedron.

Table 1: Debye temperatures and fitting parameters for the DEA low-temperature volume and the DWF fit

Data	Parameter	Al	Si	Framework	O	Na	I	Total
Volume fit, only TOF	θ_D /K							509(10)
	k_D /10^{-12}							14.4(25)
DWF	θ_{Da}	534(6)	817(5)	618(3)	513(3)	458(4)	161(3)	512(5)
	c_a	0	0	0	75(4) 10^{-5}	22.179(3)) 10^{-5}	5.1(4)) 10^{-5}	
	atomic mass /u	26.982	28.085	27.5335	15.999	22.99	126.904	
	b	1.653(7)	2.724(2)	2.237(2)	2.338(2)	1.183(6)	1	
	zero-point disorder	-	-	-	-	-	0.00080(1)	

Table 2: The components of the anisotropic displacement tensors and its isotropic equivalent calculated from PDF data

atom		T /K	U_{PDF}^{11} /10^4pm²	U_{PDF}^{22} /10^4 pm²	U_{PDF}^{33} /10^4 pm²	U_{PDF}^{12} /10^4 pm²	U_{PDF}^{13} /10^4 pm²	U_{PDF}^{23} /10^4 pm²	U_{eq} /10^4 pm²
Al		5	0.006798	0.006402	0.006509	-0.000072	-0.000126	-0.000006	0.0066
		165	0.008091	0.008061	0.008298	0.00017	0.000027	-0.000051	0.0082
		240	0.00745	0.007696	0.00751	0.000172	0.000167	0.000201	0.0076
SI		5	0.006292	0.005924	0.005085	0.000071	-0.000276	-0.000153	0.0058
		165	0.007576	0.007571	0.007518	-0.000259	0.000012	0.00016	0.0076
		240	0.002687	0.002619	0.002869	0.000088	0.000016	0.000073	0.0027
O		5	0.004976	0.004228	0.003876	-0.000059	-0.000174	-0.000004	0.0044
		165	0.004759	0.004936	0.004908	0.000001	0.000074	0.000093	0.0049
		240	0.004645	0.004562	0.004634	-0.000031	-0.000057	0.000166	0.0046
Na		5	0.006292	0.005924	0.005085	0.000071	-0.000276	-0.000153	0.0058
		165	0.007576	0.007571	0.007518	-0.000259	0.000012	0.00016	0.0076
		240	0.00694	0.007125	0.007121	-0.000175	0.000001	-0.000051	0.0071
I		5	0.010497	0.009384	0.008207	-0.000793	-0.000333	0.000018	0.0094
		165	0.011092	0.011473	0.011262	-0.000952	-0.000204	-0.001355	0.0113
		240	0.010602	0.011058	0.010975	-0.000315	0.000044	0.00066	0.0109

Supplementary Information to the article "Low-temperature anharmonicity and symmetry breaking in the sodalite $|Na_8I_2|[AlSiO_4]_6$"

by

Lars Robben[a,b]*, Isaac Abrahams[c], Michael Fischer[d], Stephen Hull[e], Martin T. Dove[f] and Thorsten M. Gesing [a,b]

g) University of Bremen, Institute for Inorganic Chemistry and Crystallography, Leobener Str. 7, D-28359 Bremen, Germany

h) University of Bremen, MAPEX Centre for Materials and Processes, Bibliothekstrasse 1, D-28359 Bremen, Germany

i) School of Biological and Chemical Sciences, Queen Mary University of London, Mile End Road, London E1 4NS, United Kingdom

j) University of Bremen, Crystallography Group, Department of Geosciences, Klagenfurter Str. 2-4 ,28359 Bremen, Germany

k) ISIS Facility, Rutherford Appleton Laboratory, Chilton, Didcot, Oxfordshire OX11 0QX, United Kingdom

l) School of Physics and Astronomy, Queen Mary University of London, Mile End Road, London E1 4NS, United Kingdom

1. Rietveld Refinement of the average structure at 5 K

The following tables provide the details of the structure refinement (table S1), atomic parameters (table S2). Rietveld plots are given in Figure S1 to S3 for detector banks 2, 3 and 5.

Table S1: Details of TOF neutron data collection and refinement of $|Na_8I_2|[AlSiO_4]_6$

Powder	White
Radiation	TOF Neutron
TOF_{min}	2000 µs
TOF_{max}	20000 µs
TOF stepwidth	1.1 µs
space group	$P\bar{4}3n$
a / pm	899.65(0)
Volume /10^6 pm³	7.2815(1)
T /K	5(1)
R_{exp}	0.79
R_{wp}	1.56
R_{Bragg}	1.21

Table S2: Atomic parameters of $|Na_8I_2|[AlSiO_4]_6$

Atom	*Site*	*x*	*y*	*z*	*occupancy*	$B_{iso}/10^4 pm^2$
Na	8e	0.19784(6)	x	x	1	0.68(1)
Al	6c	¼	½	0	1	0.35(2)
Si	6d	¼	0	½	1	0.15(1)
O1	24i	0.14182(5)	0.15106(5)	0.44794(3)	1	0.444(5)
I	2a	0	0	0	1	0.50(1)

TOF /ms

Figure S1: Results of the Rietveld refinement of $|Na_8I_2|[AlSiO_4]_6$ with observed (black upper curve), calculated (red), difference curve (black lower curve) (detector Bank 2, Polaris@ISIS).

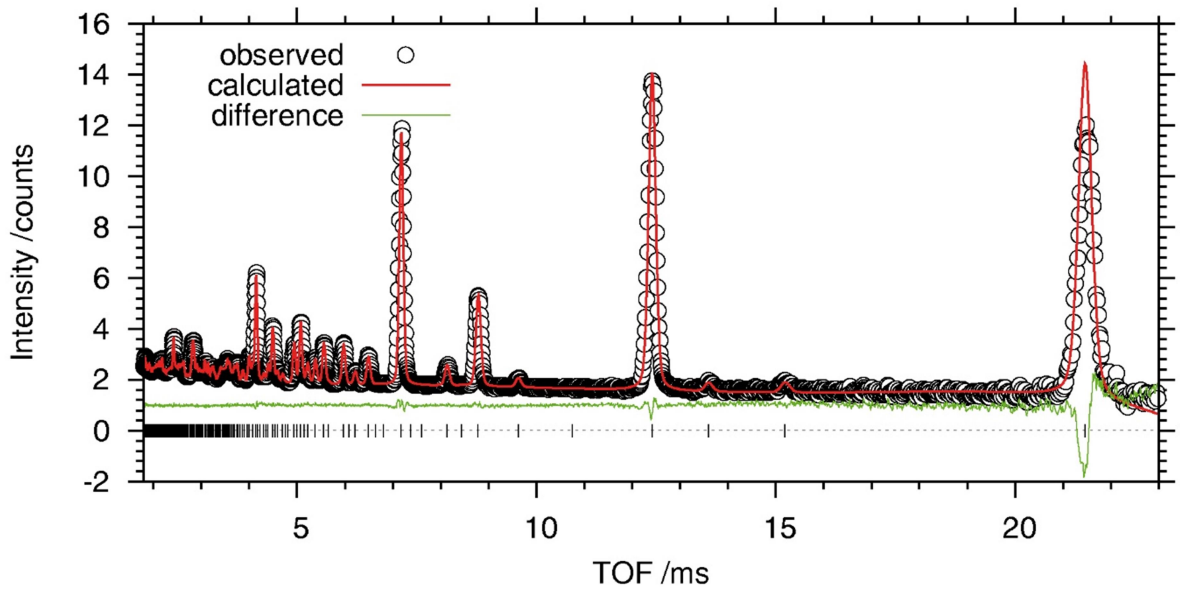

Figure S2: Results of the Rietveld refinement of $|Na_8I_2|[AlSiO_4]_6$ with observed (black upper curve), calculated (red), difference curve (black lower curve) (detector Bank 3, Polaris@ISIS).

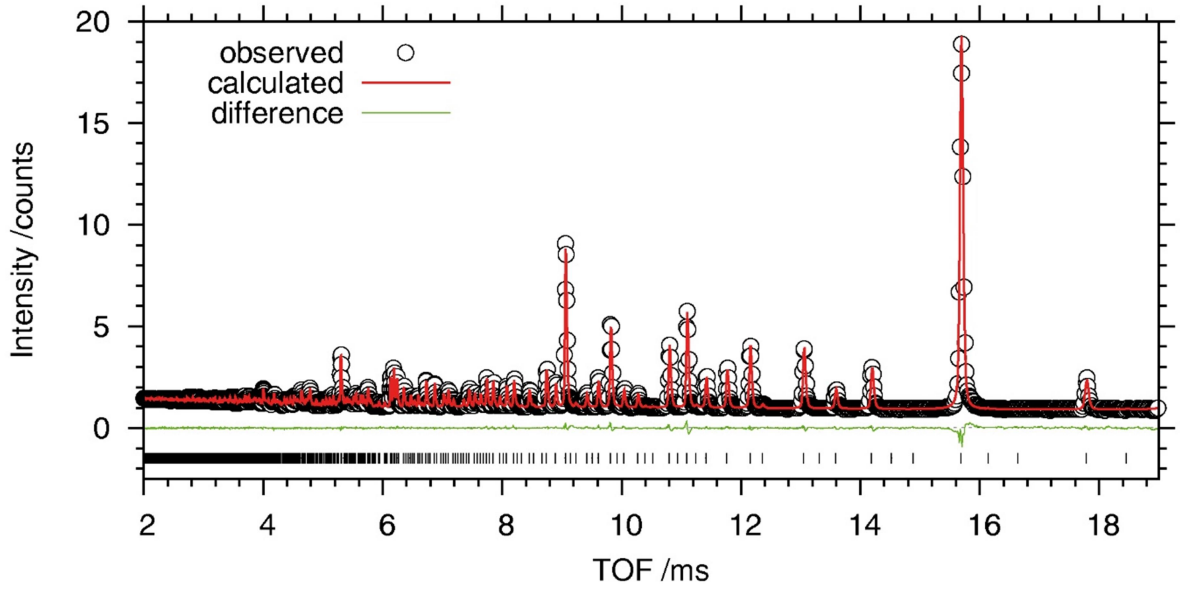

Figure S3: Results of the Rietveld refinement of $|Na_8I_2|[AlSiO_4]_6$ with observed (black upper curve), calculated (red), difference curve (black lower curve) (detector Bank 5, Polaris@ISIS).

2. TD X-ray powder diffraction and selected structural parameters from the temperature-dependent scattering

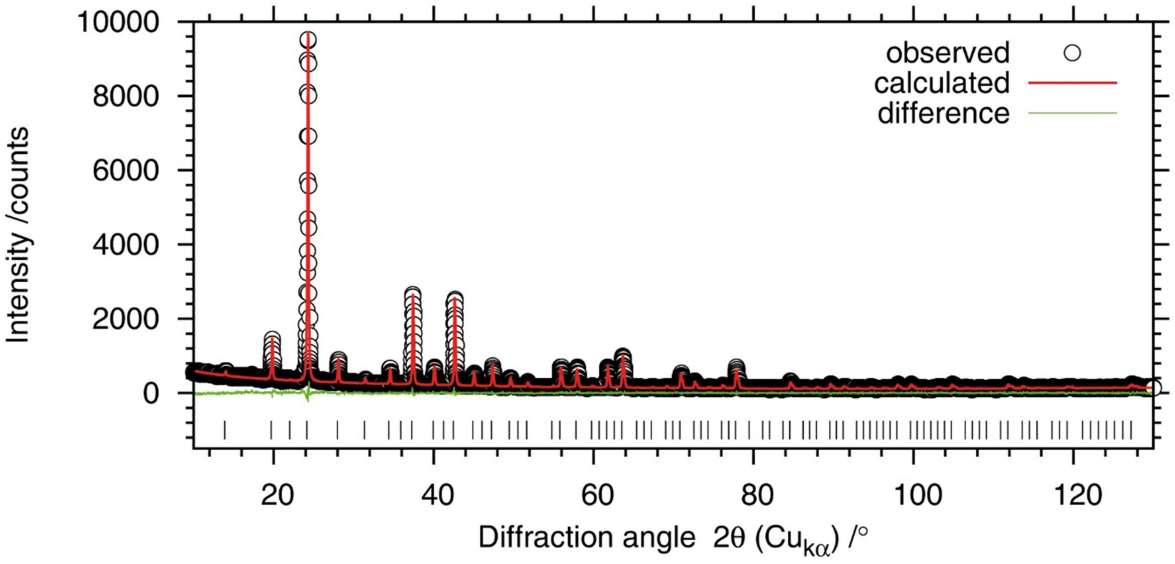

Figure S4: Exemplary refinement of data collected at 298 K

Table S3: Details of X-ray data collection and refinement of $|Na_8I_2|[AlSiO_4]_6$ at 298 K

Powder	White
Radiation	Cu (kα1, kα2)
$2\theta_{min}$	10°
$2\theta_{max}$	130°
2θ stepwidth	0.02°
space group	$P\bar{4}3n$
a / pm	902.24(2)
Volume /10^6 pm³	7.344(1)
T /K	298(1)
R_{exp}	0.65
R_{wp}	0.75
R_{Bragg}	1.26

Table S4: Atomic parameters of $|Na_8I_2|[AlSiO_4]_6$

Atom	*Site*	*x*	*y*	*z*	*occupancy*	B_{iso} /10^{4}pm²
Na	8e	0.1990(3)	x	x	1	1.1(2)
Al	6c	¼	½	0	1	0.0(7)*
Si	6d	¼	0	½	1	0.0(7)*
O1	24i	0.144(2)	0.148(2)	0.4520(4)	1	0.3(1)
I	2a	0	0	0	1	2.56(7)

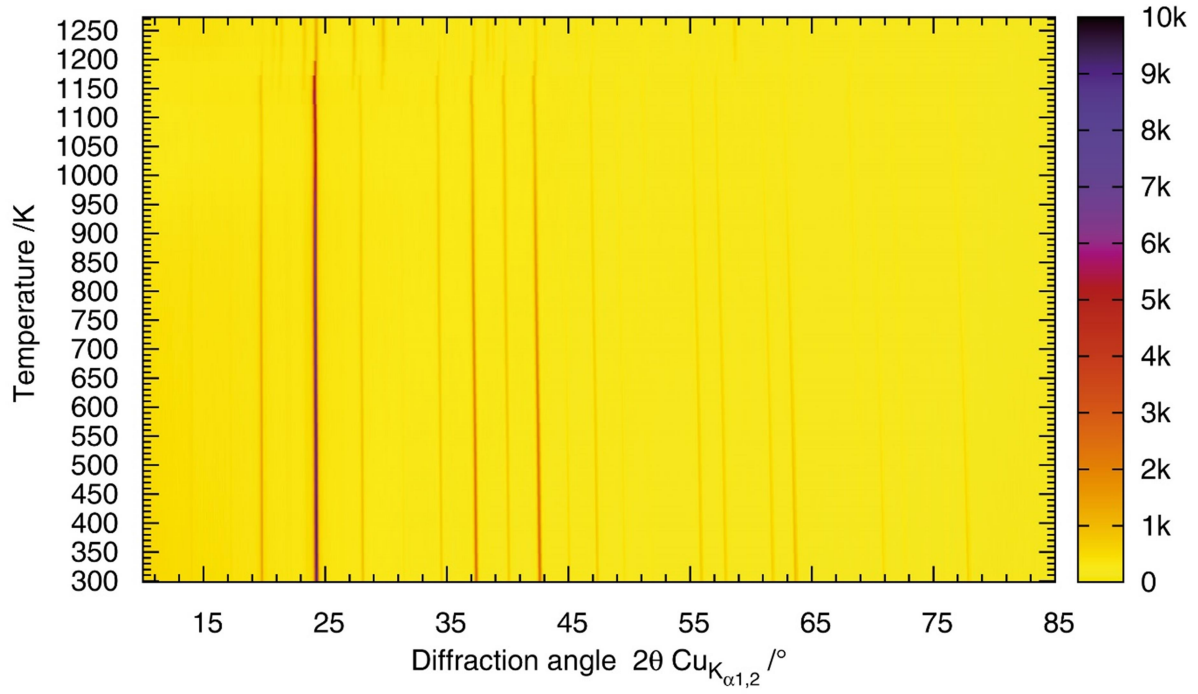

Figure S5: Complete X-ray powder diffraction temperature-dependent data

Sodalite framework tilt angle and selected mean bond distances obtained from the temperature-dependent Rietveld refinements are given in figure S4.

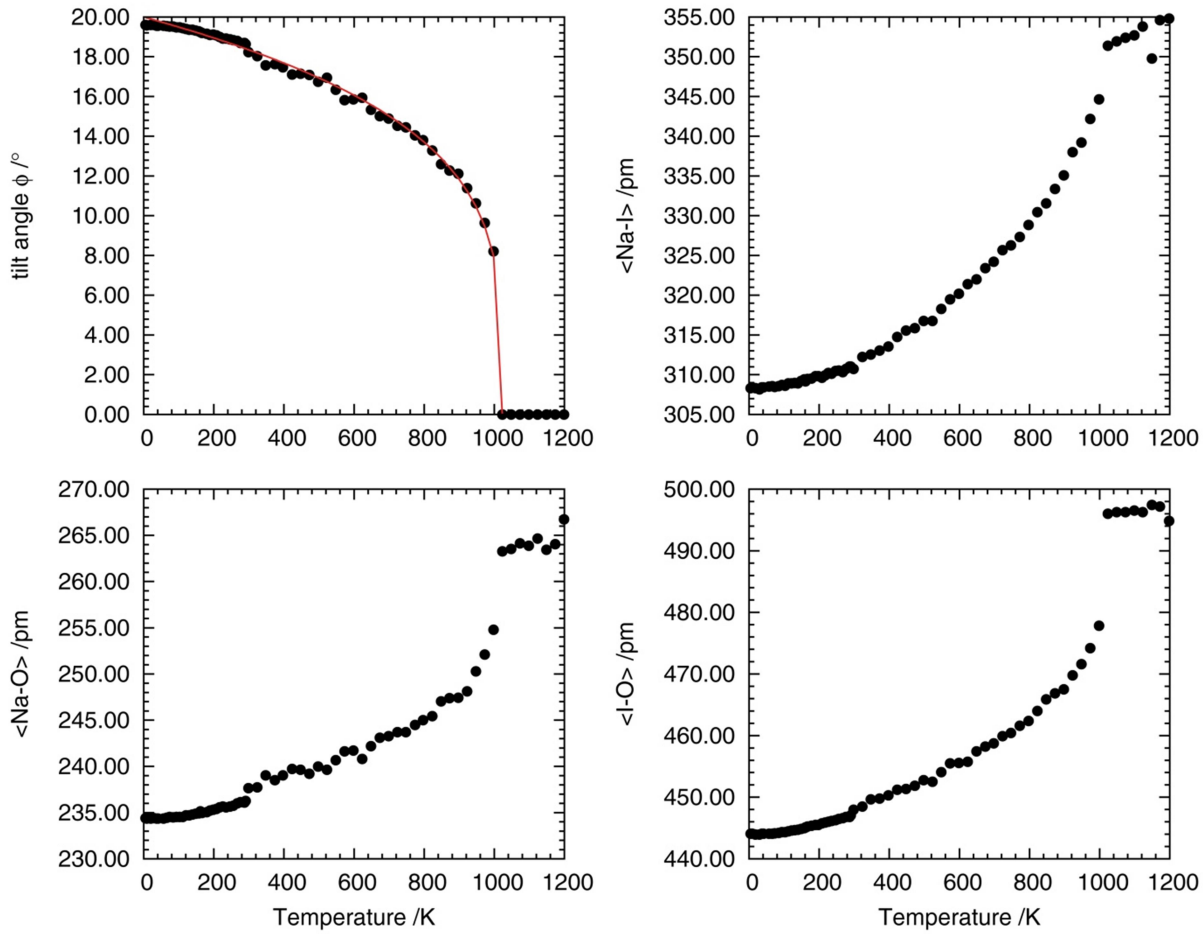

Figure S6: Mean tilt angle (with fitting of Landau type behaviour) and selected atomic distances from 5 K to 1200 K

The mean values of the distances <Na-I>, <Na-O> and <I-O> show an increasing enlargement up to approximately 1000 K followed by a linear increase at higher temperatures. This indicates the phase transition from space group $P\bar{4}3n$ to $Pm\bar{3}n$, the fully expanded state of the sodalite. This phase transition could be described within the scope of the Landau-theory using the tilt angle φ as the order parameter. The temperature of the phase-transition T_c can be determined by a least squares refinement of

$$\varphi(T) = A_0 * (1 - (T/T_c)^n \quad \text{(Equation S1)}$$

where A_0 is the correlation factor between the tilt-angle and the Landau order parameter and n the Landau exponent, resulting in T_C = 1023(2) K, A_0 = 20(1)° and n = 0.248(2) (see figure

S4, upper left panel). An exponential parameter of n = 0.25 is correlated with a tri-critical phase-transition behaviour (2-6 potential).

3. DEA Fitting of the volume thermal expansion and its coefficient $\alpha_{I,vol}(T_M)$

The temperature-dependent cell volume obtained by the Rietveld refinements up to 300 K was fitted using a Debye-Einstein-Anharmonicity (DEA) model (Figure 5) according to the formula:

$$M(T) = M_0 + \sum_{i=0}^{d} k_{Di} U_{Di}(T) + \sum_{i=0}^{e} k_{Ei} U_{Ei}(T) + \sum_{i=0}^{a} k_{Ai} U_{Ai}(T) \quad \text{Equation 12}$$

(*M*: metric parameter of interest (here: cell volume *V*), M_0 = zero pressure metric parameter at 0 K, *U(T)*: internal energies due to thermal lattice vibrations including the respective Debye (θ_D) and Einstein (θ_E) temperatures and fitting parameters representing the thermoelastic constant of the compound (k_D, k_E, k_A). Further details are given in [1] [2]. Here only a Debye quasi-harmonic (U_{Di}) term for the internal energy contributions is considered, means $d = 1$, e in Equation (1) are equal to 0 and with $a = 0$ no (high-temperature) anharmonic contribution was considered. V_0 was obtained during the respective fits as extrapolation towards 0 K. The fitting of eq. 1 against *V(T)* and *TEC(T)* (Figure S5 and upper inset of Figure S5) gave these values: V_0 = 0.72818(1) nm^3, k_D = 14.4(25) 10^{-12} GPa^{-1}, θ_D = 509(10) K.

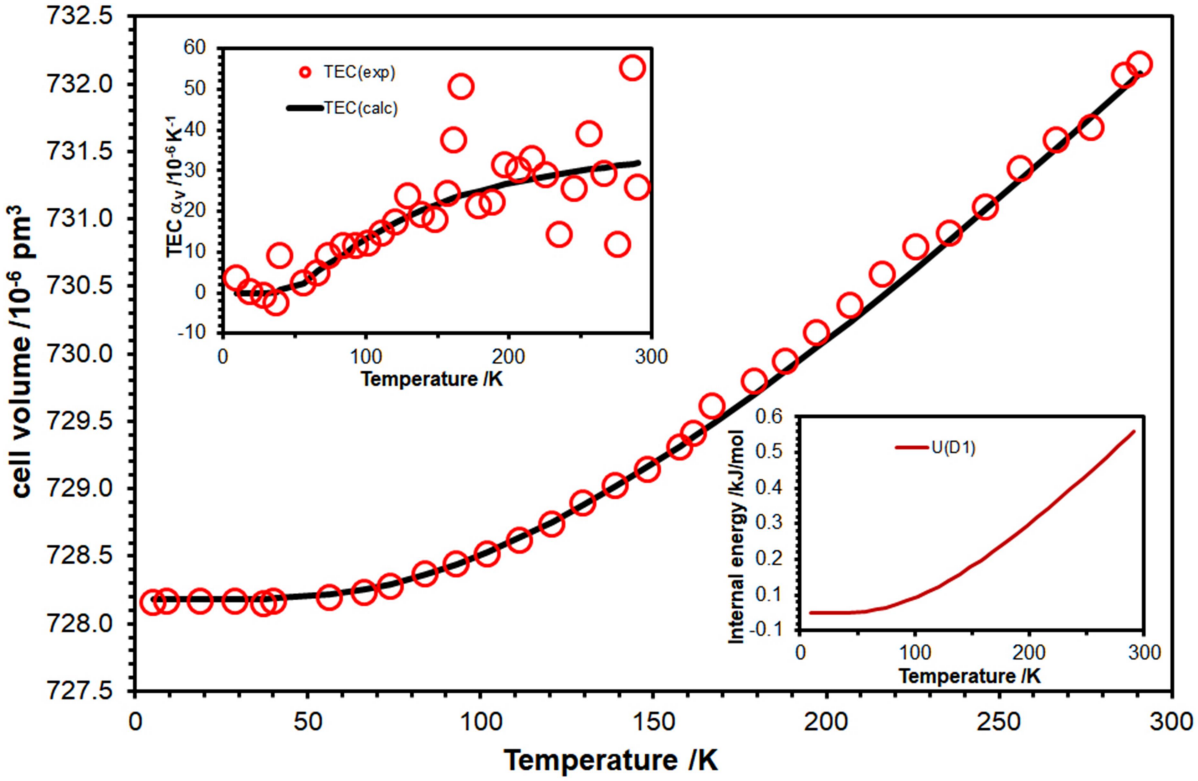

Figure S7: The DEA fit of the experimental cell volume development between 5 K and 300 K according to eq. 2. Upper inset: TEC, lower inset: internal energy.

4. MD Calculations

Molecular dynamics calculations: Dynamical aspects of the average structure

The average displacement parameters obtained from force-field MD calculations ($u_{iso,FFMD}$,Table S3) show strict linear relations with temperature and are in good agreement with the measured values. At higher temperatures the calculated values are smaller than the measured ones, because the calculations do not consider high temperature anharmonic effects. The DFT-MD calculations are based on a quasi-harmonic approximation, not considering high-temperature anharmonicity, thus the displacements temperature dependencies show a quadratic relationship. Using the displacement between calculation steps and the time resolution, the average kinetic energy (E_{kin}) of the single atoms was calculated from the FF-MD calculations.

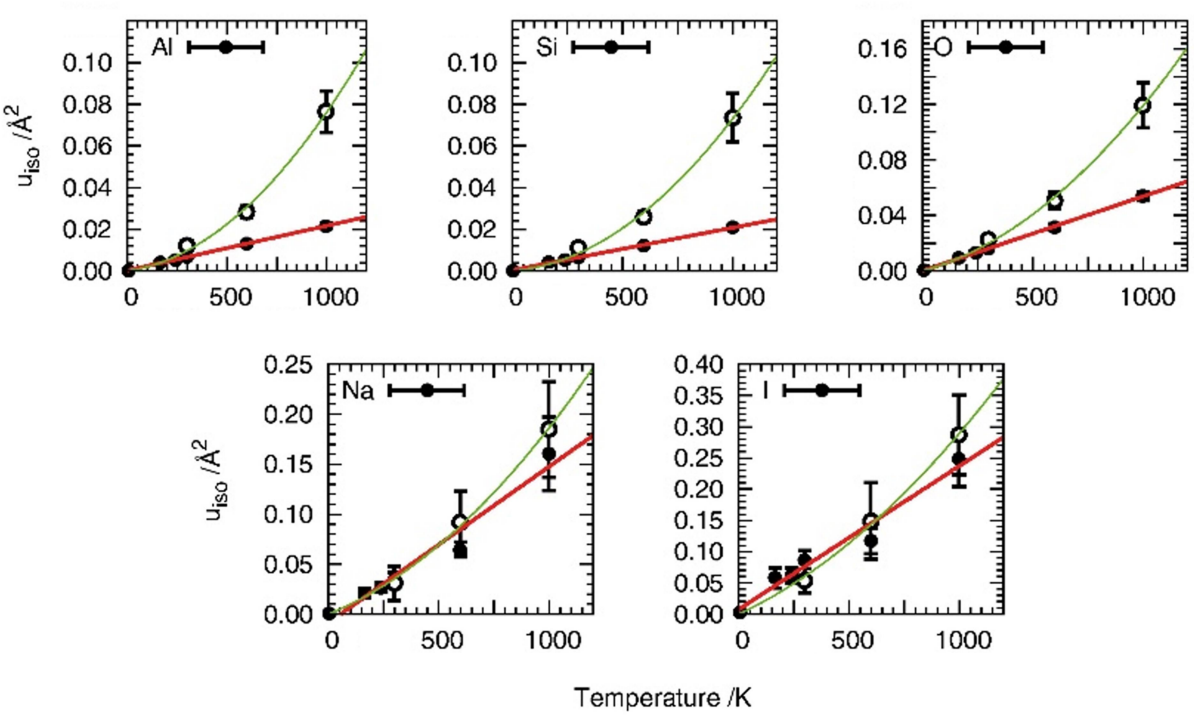

Figure S8: Mean atomic displacements u_{iso} from DFT and FF MD calculations. The lines show the results of the least-squares fitting with linear (red, FF-MD) and quadratic (green, DFT-MD) polynomials. Upper row framework atoms, lower row cage filling atoms.

Table S5: Average displacement parameters ($u_{iso,FFMD}$) and kinetic energies (E_{kin}) from FF-MD calculations

FF-MD	Al	Si	O	Na	I
T /K	$u_{iso,FFMD}$ / 10^{-10} m				
5	0.00014(2)	0.00013(2)	0.00031(5)	0.0007(2)	0.0023(9)
165	0.0040(4)	0.0042(4)	0.0094(8)	0.021(5)	0.06(2)
240	0.0053(5)	0.0055(5)	0.013(1)	0.027(5)	0.06(1)
298	0.0069(6)	0.0065(6)	0.016(1)	0.036(6)	0.09(1)
598	0.0131(8)	0.0122(8)	0.032(2)	0.065(8)	0.12(2)
998	0.022(1)	0.021(1)	0.054(3)	0.16(4)	0.25(4)
	E_{kin} /eV				
5	0.00003(1)	0.00003(1)	0.00006(1)	0.00013(1)	0.0005(3)
165	0.0012(1)	0.0012(2)	0.0019(3)	0.0040(5)	0.009(2)
240	0.0016(2)	0.0017(2)	0.0028(5)	0.0061(7)	0.010(3)
298	0.0020(2)	0.0019(2)	0.0033(6)	0.0074(9)	0.013(4)
598	0.0040(4)	0.0041(5)	0.007(1)	0.015(2)	0.019(8)
998	0.0066(6)	0.0068(8)	0.012(3)	0.024(3)	0.03(1)
Slope	$6.62\ 10^{-6}$	$6.80\ 10^{-6}$	$11.6\ 10^{-6}$	$24.5\ 10^{-6}$	$30.2\ 10^{-6}$

5. Collected atom distributions from PDF refinements

The distributions are shown in projections on the ab, ac and bc planes (from left to right). The temperatures are 5 K for the top, 165 K for the middle and 240 K for the lowest row.

5.1.Aluminium

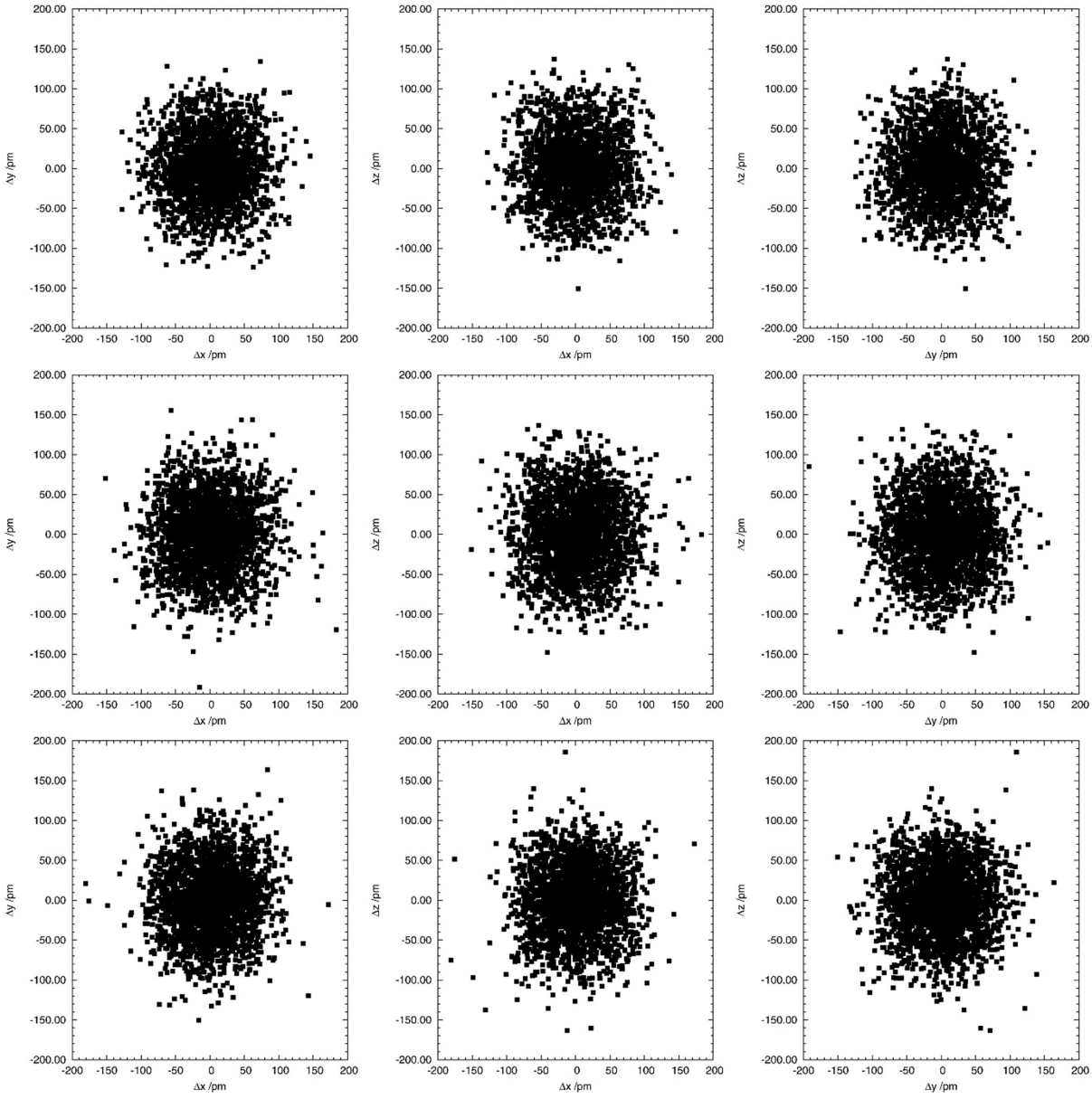

5.2.Silicon

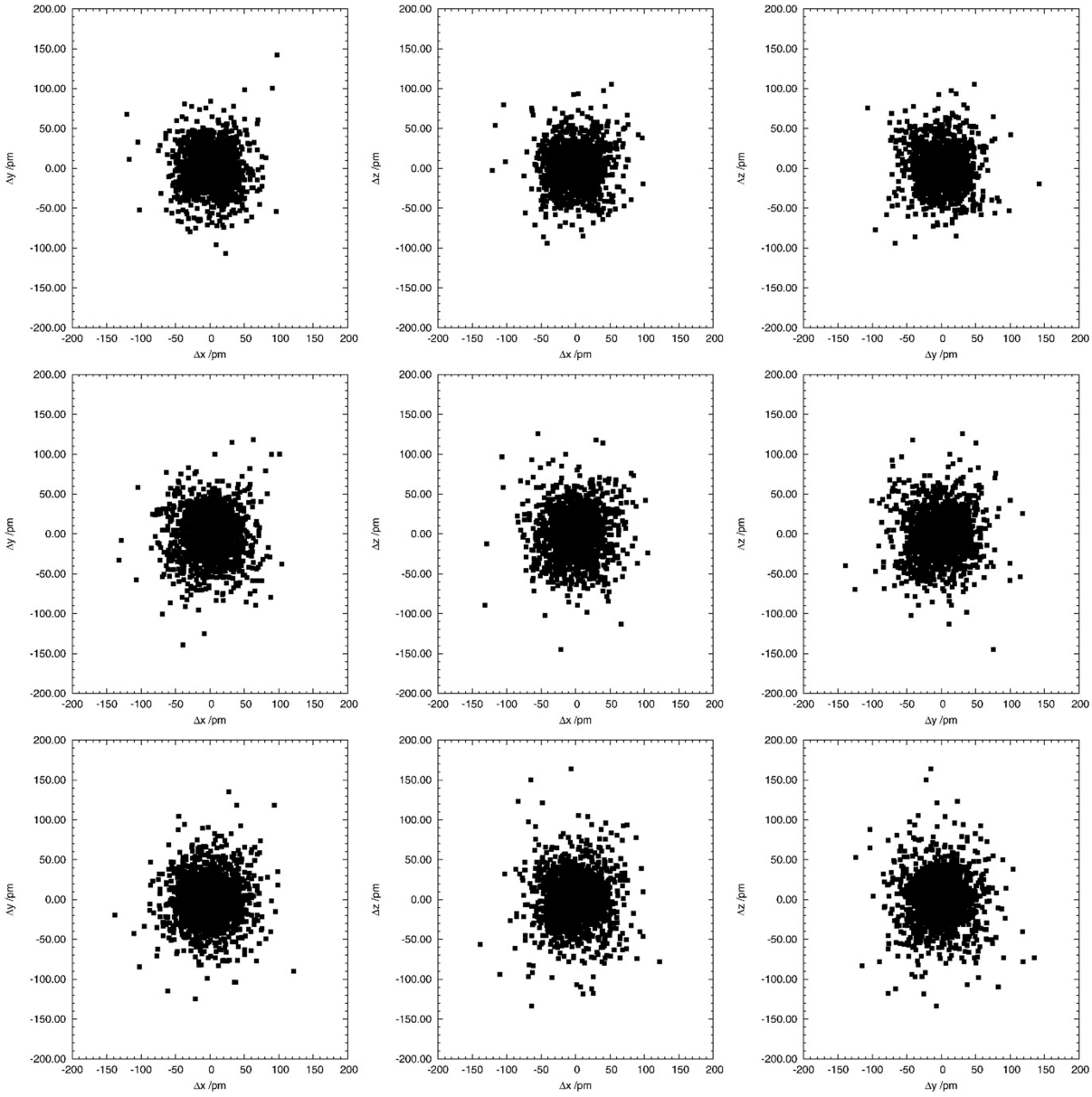
Δy /pm
Δz /pm
Δz /pm
Δy /pm
Δz /pm
Δy /pm
Δx /pm
Δx /pm
Δy /pm
200.00
150.00
100.00
50.00
0.00
-50.00
-100.00
-150.00
-200.00
-200 -150 -100 -50 0 50 100 150 200

5.3.Oxygen

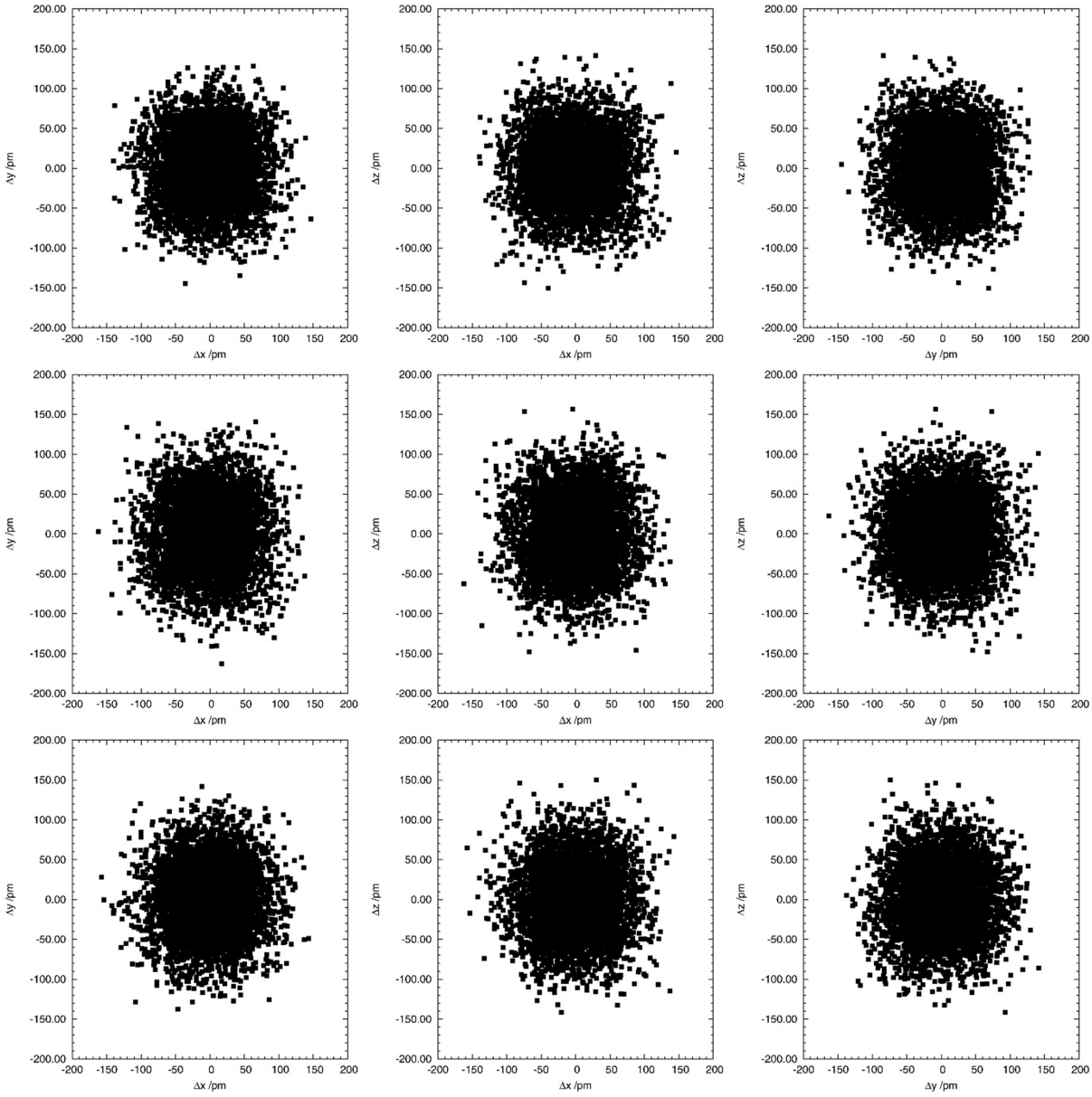
Δy /pm
Δz /pm
Δx /pm
Δy /pm
Δz /pm
Δx /pm
Δy /pm
Δz /pm
Δx /pm
Δy /pm
Δz /pm
Δx /pm
Δy /pm
Δz /pm
Δx /pm
Δy /pm
Δz /pm
Δx /pm
200.00
150.00
100.00
50.00
0.00
-50.00
-100.00
-150.00
-200.00
-200 -150 -100 -50 0 50 100 150 200

5.4.Sodium

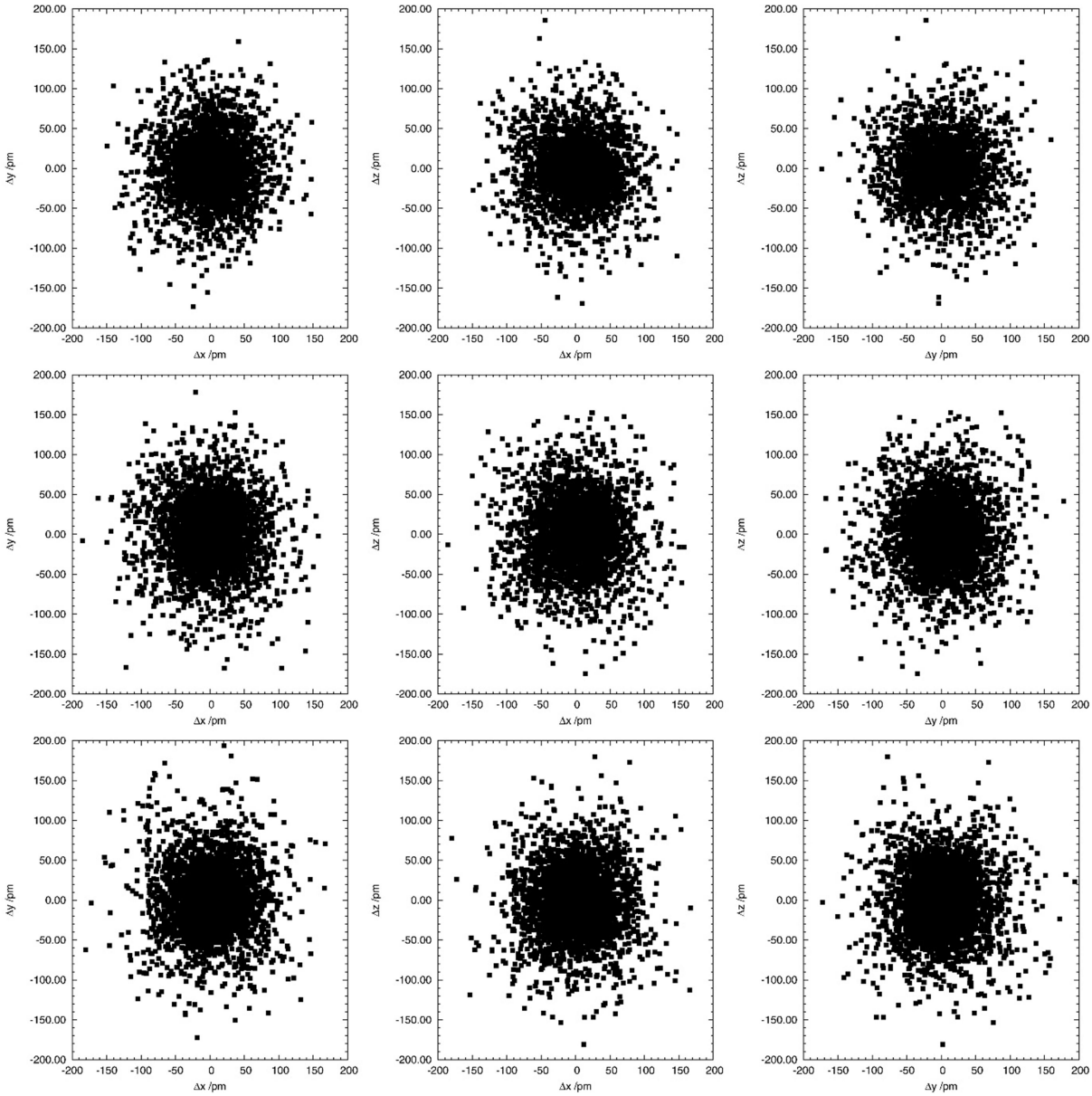
Δy /pm
Δx /pm
Δz /pm
Δx /pm
Δz /pm
Δy /pm
Δy /pm
Δx /pm
Δz /pm
Δx /pm
Δz /pm
Δy /pm
Δy /pm
Δx /pm
Δz /pm
Δx /pm
Δz /pm
Δy /pm

5.5.Iodine

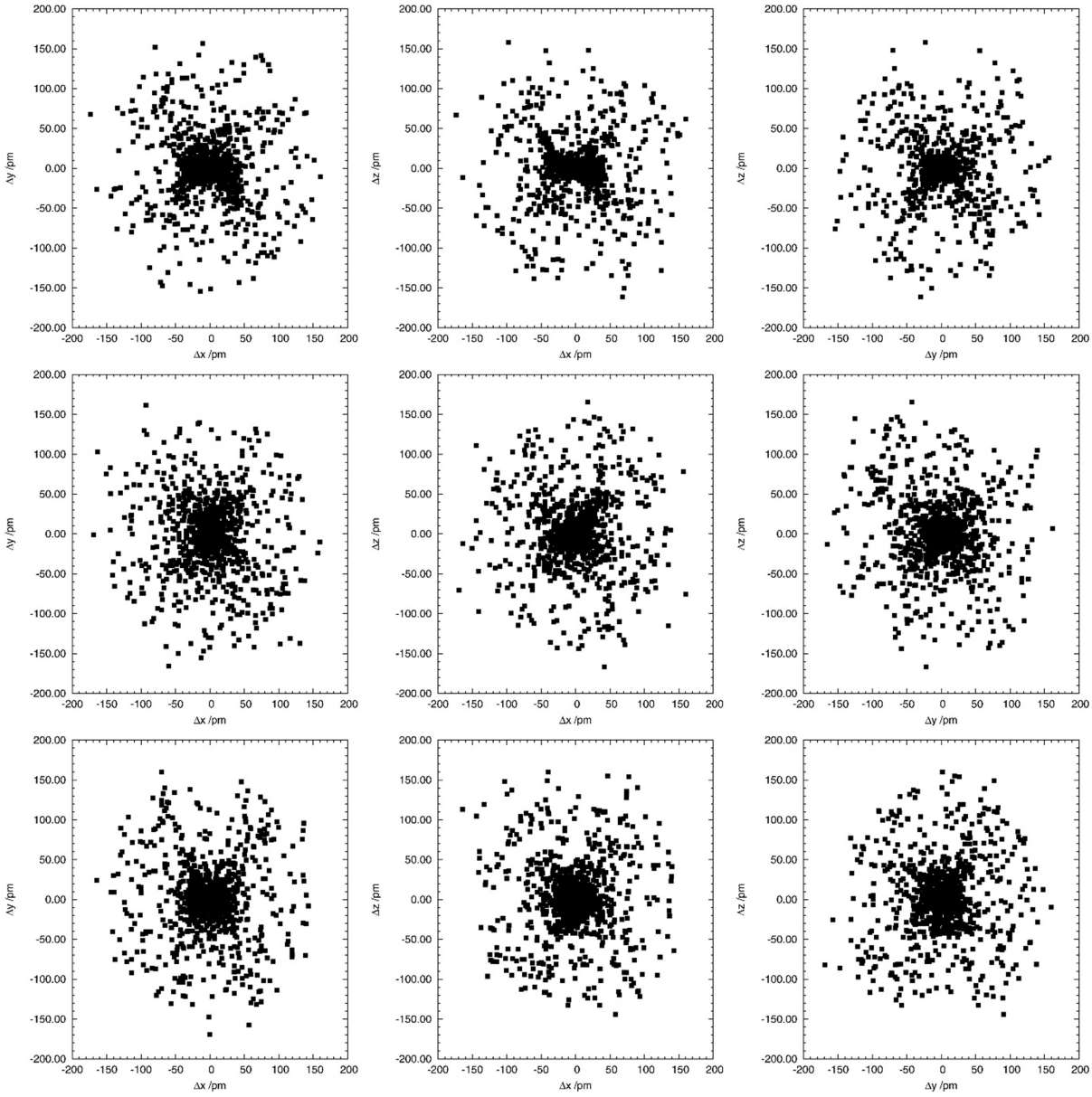
Δy /pm
Δx /pm
Δz /pm
Δx /pm
Δz /pm
Δy /pm
Δy /pm
Δx /pm
Δz /pm
Δx /pm
Δz /pm
Δy /pm
Δy /pm
Δx /pm
Δz /pm
Δx /pm
Δz /pm
Δy /pm

References SI:

[1] M.M. Murshed, C.B. Mendive, M. Curti, G. Nénert, P.E. Kalita, K. Lipinska, A.L. Cornelius, A. Huq, T.M. Gesing, *Mater. Res. Bull.* 2014, 59, 170–178.

[2] M.M. Murshed, P. Zhao, A. Huq, Th.M. Gesing, ZAAC 644 (2018) 253-259